Acta Materialia **56**(5), 1114–1125 (2008)

Fatigue of a Laterally-constrained Closed Cell Aluminum Foam

M. Kolluri[1], M. Mukherjee[2], F. Garcia-Moreno[2], J. Banhart[2], and U. Ramamurty[1*]

[1]Department of Materials Engineering, Indian Institute of Science, Bangalore-560012, INDIA

[2]Structural Research, Hahn-Meitner-Institute Berlin, Glienicker Strasse 100, D-14109 Berlin, GERMANY

Abstract

An experimental investigation into the constant stress amplitude compression-compression fatigue behavior of closed-cell aluminum foam, both with and without lateral constraint, was conducted. Results show that while the early stages of strain accumulation due to fatigue loading are independent of constraint, the rapid strain accumulation stage behaviors are sensitive to the constraint. This was ascribed to the noticeable hardening with plastic deformation observed under constraint during quasi-static loading, which in turn reduces the effective maximum stress experienced by the foam specimen during fatigue loading. This was demonstrated through a simple empirical model that connects fatigue strain accumulation without constraint to that under constraint. Complementary X-ray tomography experiments suggest that fatigue behavior of the foams is relatively less sensitive to the morphological defects such as missing walls as the quasi-static mechanical properties such as plastic strength. Evaluation of the energy absorption behavior suggests that the damage that accumulates during fatigue does not affect the energy absorbing ability of the foam adversely.

Keywords: foams; fatigue; aluminum; plastic deformation; strain accumulation

1. Introduction

Aluminum alloy foams are an important class of cellular materials that are increasingly being used for different applications such as cores of sandwich panels, crash energy absorption elements in automotive industries and several multi-functional construction

* Corresponding author. Phone: +91-80-2293-3241. Fax: +91-80-2360-0472. e-mail: ramu@materials.iisc.ernet.in

elements in vehicles for sound absorption, vibration damping and heat dissipation. This is because these materials simultaneously satisfy several design objectives such as high relative specific stiffness (vis-à-vis other types of cellular materials), high mechanical energy absorption [1-3] – that too at a constant stress giving rise to good energy absorption efficiency – and good damping characteristics with adequate mechanical strength. Components made of metallic foams are likely to be subjected to cyclic loads in many of the aforementioned applications. Therefore, the fatigue performance of this class of materials is of scientific as well technological interest. In particular, knowledge of the degradation in strength and energy absorption capability of the metallic foam as a function of the number of fatigue cycles is essential for reliable and durable design of foam containing structures.

Few studies on fatigue properties of aluminum foams have been reported in the recent past [1,4-10]. In all these studies major emphasis was put on evaluation of cyclic life under different loading conditions (compression-compression, tension-tension, etc.) [4,5], understanding of the yielding mechanisms in different length scales (macro/micro scales) [7-11] and estimation of fatigue crack propagation rates [12,13], etc. During compression-compression fatigue of metal foams, strain accumulates progressively. Sugimura et al. [4] observed that this strain accumulation occurs in three stages, which are described later in section 3.

Harte et al. [5] reported that the deformation of the foam under cyclic loading leads to loss of uniaxiality by shear band formation. In an actual application - foam filled structural elements used in automotive industries for example - deformation occurs under constrained stress state where foam is not allowed to shear in an unconstrained manner. Therefore, it becomes essential to study the foam's mechanical behavior under lateral constraint. Our recent work on quasi-static deformation behavior of a closed cell Al foam, trade name Alporas, showed that the lateral constraint induces plastic strain hardening [14]. Analytical modeling showed that two sources are responsible for this; (a) multi-axial state of stress and (b) frictional resistance between the deforming foam and the rigid constraint walls. This strain hardening is likely to influence the different stages of strain accumulation, especially stage II (incubation) and stage III (rapid strain accumulation). We have investigated this possibility in this work by conducting a comprehensive

experimental study on the fatigue of Alporas. In addition to a comparison of the unconstrained and constrained compression-compression fatigue response, we examine the micromechanical reasons for fatigue through X-ray tomography and propose a simple analytical model that connects strain accumulation under constraint due to fatigue to that without any constraint.

2. Material and Experiments

The metal foam used in this study is a commercial closed cell aluminum foam named 'Alporas' and is produced by Shinko Wire Company, Japan, in the form of 100 mm thick sheets that are 500 x 500 mm^2 in size. Manufacture of these foams involves melting the aluminum at 680°C followed by addition of 1.5wt% Ca to increase the viscosity of the melt and 1-3wt% TiH_2 as a foaming agent. Thermal decomposition of TiH_2 gives rise to H_2 that causes foaming action. Further details of manufacturing process of these foams and other relevant properties can be found elsewhere [4,15-18].

Samples of 50 x 50 mm^2 cross section and 100 mm height were prepared for mechanical testing by electro-discharge machining. In all cases, the plate thickness orientation of the foam coincides with the loading direction. Load controlled constant stress amplitude compression-compression fatigue experiments were conducted in a servo-hydraulic universal testing machine with a computer-aided data acquisition system. Each sample was tested at a frequency of 10 Hz up to 10^6 cycles. The load ratio, R (defined as the ratio of the minimum to the maximum loads of the sinusoidal fatigue cycle) was maintained at 0.1 for all the fatigue tests. Tests without constraint were conducted by simply placing the machined specimens between two parallel rigid platens of the universal testing machine. In case of tests with constraint, specimens were fixed into the steel sleeve (as shown in the Fig.1) with the help of screws (which enabled easy removal of the deformed specimens). Then an aluminum block, which has slightly smaller dimensions than the inner dimension of the steel sleeve, was used to compress the specimen within the sleeve.

Mechanical properties of the foams directly depend on their relative density, ρ^* (ratio of foam's density to the density of the constituent solid) [1,19,20]. Keeping this in mind, ρ^* of all samples used for the present work were measured (by recourse to

weight and volume measurements) before conducting any experiments. Fig. 2 shows the ρ^* of all samples and clearly indicates that even the specimens machined from the same batch tend to have a notable density distribution. Certainly this influence of ρ^* has to be accounted for when comparing the strain accumulation characteristics between different samples under fatigue loading. In the present study, each specimen has been tested at a constant maximum stress, σ_{max}, to plastic strength, σ_p, ratio. Recognizing the high variability in mechanical properties exhibited by the foams (even at the same ρ^*) [21], a minimum number of three tests were conducted at each (σ_{max}/σ_p) value for both constrained and unconstrained cases. Before conducting the fatigue tests, quasi-static compression tests were carried out on specimens from the same batch with and without constraint over a range of relative densities to obtain the σ_p values as a function of ρ^*.

Complementary X-ray tomography was performed on specimens whose cyclic loading was periodically interrupted. A microfocus X-ray source (100 kV voltage, 100 μA current and 5 μm spot size) and a flat panel detector (area 120x120 mm^2, 2240x2368 $pixel^2$, pixel size 50 μm) were used for imaging [22]. The foam was placed on a motor-controlled rotating table with the height of the foam perpendicular to the X-ray beam direction. The foam was rotated by one degree at a time around its vertical axis and a radioscopic projection of the foam was taken after each rotation with an exposition time of 8 s. A total of 360 projections were taken for a complete rotation of the foam. After this, tomographic cone beam reconstructions were performed on these 360 projections using the commercial software Octopus 8.1. After reconstruction, another commercial software VGStudioMax 1.2.1, was used to visualize the 3D volume of the foam and to extract the vertical sections of the foam.

A self-developed radioscopic image analysis software AXIM was used to calculate the density variation across the foam at different strain levels by analysing radioscopic projections [22]. AXIM can calculate the intensity variation across the foam, which can be correlated to the density of the foam. While taking projections, the orientation of the foam was kept constant so that the undeformed parts of the foam at different strain levels appear similar in the projections. An area of 100 pixels wide (50 pixels wide on both sides of the central vertical axis of projection) was chosen along the height of the foam and an intensity calculation was performed on this area. The height of

the foam decreases with increasing strain level. This was compensated by rescaling the height.

3. Results of mechanical tests

3.1. Quasi-static compression

Before presenting the fatigue results – which is the main focus of the present paper – it is helpful to first briefly mention the quasi-static stress-strain response of the closed cell foam under compression, since this forms the baseline for fatigue behavior. A comparison of the typical compressive stress-strain responses obtained with and without constraint (see Fig. 3(a) of Ref. 14) shows that the elastic and initial plastic deformation behaviors are independent of the constraint. Both the responses exhibit an initial stress maximum after the elastic deformation. This first maximum, taken as the plastic strength, σ_p, increases with ρ^* (see Fig. 4(a) of Ref. 14). It is worth noting here that σ_p is independent of the constraint. Prior work [1,14,23] has shown that σ_p approximately varies with $(\rho^*)^{1.5}$ which is also true in this case. A power law fit of the following form was used in determining a σ_p value for any given ρ^*:

$$\sigma_p = A.(\rho^*)^{1.5}. \qquad (1)$$

with A = 60.92 ± 1.3. Eqn. 1 was employed to estimate the σ_p value for each of the fatigued specimens with the prior knowledge of their ρ^*.

Upon further loading beyond σ_p, significant differences between the constrained and unconstrained samples emerge. While the latter show the typical long plateau in stress with strain, the laterally constrained specimens exhibit plastic strain hardening.

3.2. Strain accumulation under cyclic loading

A key feature of compression-compression fatigue in metal foams is the progressive strain accumulation, which leads to shortening of the specimens during fatigue. This was quantified by plotting accumulated strain, ε_a, vs. number of fatigue cycles, N. Fig. 3a shows a typical variation of ε_a with N at $(\sigma_{max}/\sigma_p) = 0.9$ for specimens with and without constraint. In both the cases, three different stages in the ε_a vs. N plot can be seen. In

stage I, rapid strain accumulation within the first few cycles (N<50) of fatigue is noted. This is followed by stage II where large numbers of cycles elapse with little strain accumulation. Then at a critical number of cycles, N_c, the strain starts to accumulate rapidly again (stage III). These general trends are similar to those observed by Sugimura et al. for Alporas [4], who also identified 3 distinct stages of fatigue.

In both the constrained and unconstrained cases, ε_a at the end of the stage I is similar. Also, the onset of stage II occurs at about the same N. However, marked differences are seen in N_c, with stage III getting initiated relatively earlier in the unconstrained samples followed by a rapid rise in ε_a. This continues till the densification strain of the material, ε_d, is reached. In the case of constrained sample, stage III is not a continuous process, but is intervened by periodic slow strain accumulation. These differences are illustrated in Fig. 3b which shows the rate of plastic strain accumulation per cycle, $d\varepsilon_a/dN$, as a function of ε_a. In this figure, the onset of stage III is marked by the first minimum in $d\varepsilon_a/dN$. This minimum is ~9×10^{-6} per cycle for the unconstrained specimen and ~3×10^{-6} per cycle for the constrained one. After these minima, $d\varepsilon_a/dN$ increases again to reach a maximum of ~7×10^{-5} and ~2×10^{-5} per cycle, respectively. At this juncture, a strain jump is seen for both the cases. Here afterwards, $d\varepsilon_a/dN$ remains fluctuating within a narrow range (between 2×10^{-5} and 1×10^{-4} per cycle) for the unconstrained samples. In the constrained samples, it decreases continuously, albeit with relatively large fluctuations, with ε_a reaching a value of ~5×10^{-8} per cycle at $\varepsilon_a \approx 40\%$. Note that this is almost three orders of magnitude smaller than the corresponding $d\varepsilon_a/dN$ observed in the unconstrained case for the same ε_a.

The influence of σ_{max}/σ_p on the fatigue strain accumulation characteristics of unconstrained and constrained samples is illustrated in Figs. 4a and 4b, respectively. In both cases the N_c decreases with increasing stress level. Figs. 5a and 5b show $d\varepsilon_a/dN$ vs. ε_a plots for unconstrained and constrained specimens respectively. Local minima were observed in all the plots, except for those tested at $\sigma_{max}/\sigma_p = 0.6$. The strain corresponding to this first minimum, ε_T, which denotes the transition from stage II to stage III, remains invariant at ~3% for the unconstrained fatigue tests. The steady state strain accumulation rates in this case appear to depend on the applied stress level, increasing with σ_{max}/σ_p.

The specimens that were constrained from lateral deformation, in contrast, show an increasing ε_T with σ_{max}/σ_p, but appear to merge asymptotically at higher strains. The large oscillations observed in the $d\varepsilon_a/dN$ vs. ε_a curve in the case of constrained specimens (Fig. 5b) indicates that there are intermediate incubation periods followed by rapid strain accumulation in stage III deformation. However, it should be noted that stage III in the constrained specimens is not a *rapid strain accumulation stage* per se. This is because strain accumulation rates decrease continuously to reach levels that are even less than accumulation rates observed during incubation period (stage II) as shown in Fig. 5b. This is an example of some basic differences in the fatigue strain accumulation in constrained and unconstrained specimens.

3.3. Fatigue life

Since the fatigue tests were conducted under compression-compression cyclic loading, specimens undergo large plastic deformations and will never experience a final failure. Hence a suitable failure criterion on the basis of ε_a is necessary to construct stress vs. number of cycles (S-N) curves that will be useful in stress-life design approaches. We have considered the possibility of number of cycles at ε_T as the failure criterion, but it proved to be difficult to assess objectively as the transition from stage 2 to 3 is not sharp in the constrained samples. Banhart et al. [6] use 10% as the failure strain for this purpose whereas Zhou et al., [7] used 4% for open cell foams with a particular kind of strain accumulation behavior (type II). We employed both 4% as well as 10% for failure strain definitions. Note that the former occurs typically before the onset of stage III whereas the latter is in stage III. Employing these, the normalized maximum stress of the fatigue cycle, σ_{max}/σ_p, vs. the number of cycles to failure, N_f, curves were constructed. These are plotted for both the unconstrained and the constrained cases with 4 and 10% failure strains in Figs. 6a and 6b, respectively.

As is the case with the mechanical properties of the metal foams – despite Alporas being one of the better commercially available foams with respect to uniformity in cell sizes, etc. [21] – a large scatter in the data is seen. In general, it appears that the scatter decreases with decreasing stress amplitude.

Fig. 6 suggests that the endurance limit, taken at 10^6 cycles, is within 0.6 to 0.7 σ_{max}/σ_p range for both the constrained and unconstrained loading conditions. For higher strain of failure of 10%, (Fig. 6b), the average N_f is slightly higher vis-à-vis the unconstrained case at high stress levels. But this difference in fatigue life diminishes at low σ_{max}/σ_p values. However, the ε_a vs. N curves (Fig. 4) of the constrained and unconstrained cases diverge significantly in stage III and hence the fatigue lives are likely to be significantly different if higher strains are taken as failure limits.

4. Discussion

4.1 Mechanisms of fatigue

Under constraint, the Alporas samples exhibit plastic strain hardening, which is due to the following two factors [24]; (a) the multi-axial state-of-stress that prevails in the foam specimens due to the presence of the constraint, and (b) the friction between the deforming foam and the constraining walls. Even though the general trends observed in three stages of deformation look similar in both unconstrained and constrained cases (Fig. 3a), certainly there are some disparities in strain accumulation characteristics in stage II and stage III. This is clear from the observation of relatively prolonged incubation period (stage II) in the constrained specimens and large differences in the ε_a with increasing N (Fig. 3a).

Figs. 7a and 7b are SEM images from specimens that were fatigued with constraint to an accumulated strain of 4%, which show the presence of few large cracks and many small cracks in the cell walls. The presence of fatigue striations on the fracture surface of these cracks (Fig. 7d) together with the observation of highly degraded cell walls confirms the fact that these cracks are initiated and propagated by fatigue loading. In contrast, no cracks were observed in a specimen that was strained to a similar level, but under quasi-static loading (Fig. 7c). The cracks observed in the cell membranes are the main causes for cyclic softening as these cracks eventually grow large enough to reduce their contribution to plastic resistance. The observations made on fatigue loaded specimen with constraint in this work are similar to those made by Sugimura et al [4] on Alporas specimens subjected to compression-compression fatigue but without any constraint. Therefore, it appears that the micro-mechanisms of fatigue crack initiation and

propagation do not get altered significantly by the introduction of a lateral constraint for plastic deformation.

The reduction in the scatter of fatigue life data with decreasing stress amplitude (Fig. 6) can be inferred as following. It is fairly well established in the literature that the elastic as well as early plastic deformation (i.e. σ_p) of metallic foams are sensitive to the morphological defects such as wiggles in the cell walls, Plateau borders, and missing cell walls, common to the stochastic cellular structure of them [19,21,25,26]. The defect distribution and orientation (with respect to the loading directions), etc., in turn imparts a large variability to the quasi-static mechanical properties of the metal foams [27]. The reduced variability at the lower σ_{max} then implies that the morphological defects do not exert the same influence upon fatigue strain accumulation. The tomographic observations, presented below, are in good agreement with this hypothesis.

Turning attention to the macro-scale strain accumulation mechanisms, namely the progressive cell-band collapse mechanism, observation of the strain jumps in Fig. 8 confirms cyclic deformation under compression with constraint is also by collapse band formation. To examine this possibility as well as the internal deformation of the foam in detail, we performed X-ray computer tomography analyses on samples tested with constraint by interrupting the fatigue test at different strain values. Figs. 9 and 10 show a series of binarised images taken at different levels of plastic strains. While Fig. 9 shows the images obtained from a specimen that was deformed under quasi-static loading, Fig. 10 shows those obtained from the specimen subjected to fatigue loading. These images clearly illustrate that deformation proceeds through collective cell collapse [1,5,28] and this is true irrespective of the type of loading – quasi-static or cyclic. However, there appears to be some difference in terms of the origin of cell band collapse. In the case of quasi-static loading, plastic deformation appears to originate at large cells – more precisely where several cell walls are missing. Deformation under cyclic loads, in contrast, does not appear to be sensitive to the presence of relatively large cells. This is consistent with the relatively less scatter we observe in fatigue lives, especially at low stress amplitudes (see Fig. 6 and the comments made there off). This is in complete contrast to fully dense (or solid) metals and alloys, where fatigue life is far more sensitive to pre-existing defects than quasi-static properties.

Further support for this has been obtained through the mechanical energy absorption measurements. One of the key attributes of metal foams is their ability to absorb large amounts of energy during deformation by virtue of a long stress plateau [1,23]. In the context of fatigue, a key issue that has not been examined in the limited literature on fatigue of metal foams that is available hitherto, is the following: *Does damage accumulated during fatigue adversely affect their energy absorption capability*? To address this, we subjected fatigued specimens with $\varepsilon_a \sim 6$ % to quasi-static compression tests and evaluated the densification strain, ε_d, and energy absorbed per unit volume, W, using the procedures outlined in references [14,29]. Fig. 11a shows that the ε_d in fatigued specimens is smaller vis-à-vis those of the specimens of similar relative density but did not experience any fatigue loading prior to quasi-static compression. This is due to the obvious reason that in the former case, some of the total allowable ε_d was already consumed during fatigue. Note that the difference between ε_d of these cases is approximately 6%, similar to ε_a due to fatigue.

In Fig. 11b, we compare the specific energy absorbed, W, as a function of the relative density. The values of W for the fatigue cases were calculated using the specimen height at the beginning of the quasi-static tests, i.e., the strain is taken as zero at the beginning of the quasi-static tests of the fatigue specimens. (Note that the cross-section hardly changes during deformation). Clearly, Fig. 11b shows that there is no additional energy loss *per-se* due to fatigue, with the fatigued specimen data falling on top of those that did not see any fatigue. While it is likely that there is some damage induced during fatigue, in terms of cracked cell walls, etc., they do not appear to be contributing to the loss in energy absorbing ability. This is simply because cell walls play relatively minor role in the plastic deformation during the quasi-static loading (as evidenced by the $(\rho^*)^{1.5}$ fit to the plastic strength). Note that W approximately scales with the product of ρ^* and σ_p. A natural extension of this argument is that scaling of remnant energy absorbing ability of fatigued specimens can be made with reasonable confidence. For example, if a component made of foam experiences fatigue with an ε_a of say 20%, its energy absorption capability will be 80% of that a pristine specimen.

Fig.12a shows the variation of the localized relative density with the rescaled length in a sample that was subjected to deformation under quasi-static loading. Here, the

rescaling of length was necessary in order to compensate the reduction in the height of the specimen due to plastic straining. Fig. 12a clearly suggests that under quasi-static loading, the cell-collapse bands form at random locations and one densified region does not pre-determine as to where the next one forms. Fig. 12b suggests that, in contrast, cyclic loading leads to progression of deformation from the first region of collapse to its nearest neighbor and so on.

4.2 Connection between constrained and unconstrained strain accumulation

The results presented in section 3 show that the strain accumulation behavior of constrained and unconstrained specimens differ significantly in stage III. We propose that it is due to strain hardening under constraint and perform modeling in this section.

Our previous studies [14,24] on deformation of foams under lateral constraint show that the plastic part of the stress-strain response of the foam has a positive slope to it, i.e., the foam strain hardens. The hardening rate, $d\sigma/d\varepsilon$, varies approximately linearly within the 7.5 to 12% ρ^* range, with a slope of ~53.22 MPa. We have conducted extensive analysis to identify the possible reasons and concluded that hardening is due to the multi-axial stress state experienced by the foam under constraint. The friction between foam specimen surfaces and the constraint walls also plays a role. However, in the case of fatigue loading, friction is unlikely to play a major role for the following two reasons. (a) The relative sliding of the specimen surface against the constraint walls in each fatigue cycle is small vis-à-vis that experienced during monotonic loading. (b) Repeated relative sliding is likely to decrease friction gradually with cycling. Our experience during fatigue testing supports this argument. While we could remove the foam specimens from the constraint jig with ease (by simply sliding the specimen out), the extraction of specimens tested under quai-static loading required dismantling of the jig by unscrewing the walls.

During fatigue, as the strain accumulates and densification proceeds with the number of fatigue cycles, the apparent macroscopic flow stress, σ_p^a, of the foam specimen increases in constrained specimen as a function of the accumulated strain, ε_a. Note that since σ_p occurs at about 5% strain, this will be true only for ε_a higher than 5%. Since the applied maximum stress, σ_{max}, is fixed during constant stress amplitude fatigue

experiments of this study, the constrained specimen effectively experiences a continuously reducing normalized maximum stress (σ_{max}/σ_p^a) value as stage III of fatigue deformation continues. For example, an ε_a = 10% makes the (σ_{max}/σ_p^a) ~ 0.8 whereas the starting (σ_{max}/σ_p) = 0.9. This effective reduction in stress experienced by the foam, in turn, leads to a continuous reduction in the strain accumulation rates assuming that the mechanisms of fatigue remain the same.

Next, the unconstrained strain accumulation curves between 5 to 20% strain was described with a power law (fits shown in Fig. 4a)

$$\varepsilon_a = K \cdot N^n \tag{2}$$

where n and K are power law exponent and coefficient respectively. It was observed that n is ~ 0.9 ± 0.05 for all stress ratios (σ_{max}/σ_p) ranging from 0.7 to 0.9. Hence, only K is function of (σ_{max}/σ_p). Variation of K with σ_{max}/σ_p is plotted in Fig. 13, suggesting a functional relationship of the form

$$K = C \cdot e^{\left[q\left(\frac{\sigma_{\max}}{\sigma_p} \right) \right]} \tag{3}$$

with C and q as fitting parameters. Best fit through the data gives C = 6.419E-12 and q =18.148. By combining Eqs. 2 and 3, the strain accumulation under fatigue loading with constraint can be written as

$$\varepsilon_a = 6.419 \times 10^{-12} \cdot e^{\left[18.148 \left(\sigma_{\max} / \left(\sigma_p + \int_0^{\varepsilon_a} \frac{d\sigma}{d\varepsilon} d\varepsilon \right) \right) \right]} \cdot N^{0.9} \tag{4}$$

Predicted variations of ε_a with N under constraint for different values of σ_{max}/σ_p are plotted in Fig. 4b along with the experimental data. Excellent agreement was found between experiment and prediction, except for the case of σ_{max}/σ_p =0.7. This suggests that

the strain hardening observed under compression has an effect in increasing the life of the specimens under fatigue loading by progressive decrease in the strain accumulation rates with deformation. This also indicates that the presence of intermediate incubation periods in stage III deformation are a consequence of the reduction in the normalized maximum stress with deformation under constraint.

5. Summary

Strain accumulation occurs during constant stress amplitude compression-compression fatigue loading of closed-cell Al foam, Alporas, with or without lateral constraint. While the first two stages are similar for constrained and unconstrained cases, the incubation period is slightly longer and the strain accumulation rates in stage III (rapid strain accumulation stage) are much smaller in specimens that were constrained from deforming laterally. Closer examination reveals that stage III under constraint contains pronounced fluctuations in strain accumulation rates. In both the cases, no fatigue effects (strain accumulation) was observed when the maximum stress of the fatigue cycle is 60% of the quasi-static plastic strength of the foam. Stress-life diagrams, constructed with two different critical strain accumulation failure criteria (4 and 10%), show a marginal improvement of fatigue life under constraint when failure strain is defined as 10%. Tomography observations on intermittently interrupted fatigue specimens suggest that the fatigue performance, especially at lower stress amplitudes, are less sensitive to the morphological defects such as large cells vis-à-vis quasi-static mechanical properties. Fatigue loading does not affect the energy absorbing capabilities of the foam, except that it can consume some of the strain (through the fatigue strain accumulation) that is otherwise available for accommodating plastic straining during the plateau part of the quasi-static stress-strain response. A simple empirical connection was made between the stage III accumulation rates of unconstrained and constrained fatigue loadings to illustrate that slower rates in the latter case are due to the reduction in effective maximum stress of the fatigue cycle, which occurs due to strain hardening observed under constraint.

Acknowledgements

UR and MK are grateful to Mr. S. Sasidhara and Mr. K. Eswar Prasad for their assistance in conducting the fatigue experiments and SEM work reported in this study. This work at IISc was funded by a grant from the Aeronautical Research & Development Agency, Defence Research and Development Organization, Government of India.

References

[1] Gibson LJ, Ashby MF. Cellular solids – structure and properties. Cambridge: Cambridge University press; 1997.

[2] Ramachandra S, Sudheer Kumar P, Ramamurty U. Scrip Mat 2003; 49: 741.

[3] Sudheer Kumar P, Ramachandra S, Ramamurty U. Mat Sci Eng A 2003; 347: 330.

[4] Sugimura Y, Rabiei A, Evans AG, Harte AM, Fleck NA. Mat Sci Eng A 1999; A269: 38.

[5] Harte AM, Fleck NA, Ashby MF. Acta Mat 1999; 47:2511.

[6] Banhart J, Brinkers W. J Mat Sci Let 1999; 18: 617.

[7] Zhou J, Soboyejo WO. Mat Sci Eng A 2004; A369: 23.

[8] Amsterdam E, De Hosson J Th M, Onck PR. Acta Mat 2006; 54: 4465.

[9] Zhou J, Gao Z, Cuitino AM, Soboyejo WO. Trans ASME 2005; 127:40.

[10] Zettl B, Mayer H, Stanzl-Tschegg SE. Int J Fat 2001; 23: 565.

[11] Bastawros AF, Bart Smith H, Evans AG. J Mech Phy Sol 2000; 48:301.

[12] Olurin OB, McCullough KYG, Fleck NA, Ashby MF. Int J Fat 2001; 23:375.

[13] Motz C, Friedl O, Pippan R. Int J Fat 2005; 27: 1571.

[14] Kolluri M, Karthikeyan S, Ramamurty U. Met Mat Trans A 2007; 38: 2006.

[15] Ramamurty U, Kumaran MC. Acta Mat 2004; 52: 181.

[16] Paul A, Seshacharyulu T, Ramamurty U. Scrip Mat 1999; 40: 809.

[17] Akiyama S, Ueno H, Imagawa K, Kitahara A, Nagata S, Morimoto K, Nishikawa T, Itoh M, Foamed metal and method of producing the same, US Patent 4,713,277, 1987.

[18] Banhart J. Prog Mat Sci 2001; 46: 559.

[19] Andrews E, Sanders W, Gibson LJ. Mat Sci Engg A 1999; A270: 113.

[20] Simone AE, Gibson LJ. Acta Mat 1998; 46: 2139.

[21] Ramamurty U and Paul A. Acta Mat 2004; 52:869.

[22] Garcia-Moreno F, Fromme M, Banhart J. Adv Eng Mater 2004; 6: 416.

[23] Ashby MF, Evans AG, Fleck NA, Gibson LJ, Hutchinson LW, Wadley HG. Metal foams: a design guide. Oxford UK: Butterworth-Heineman; 2000.

[24] Karthikeyan S, Kolluri M, Ramamurty U. Met Mat Trans A 2007; 38: 2014.

[25] Chen C, Lu TJ, Fleck NA. J Mech Phy Sol 1999; 47: 2235.

[26] Sugimura Y, Meyer J, He MY, Bart-Smith H, Grenstedt JL, Evans AG. Acta Mat 1997;45:5245.

[27] Simone AE, Gibson LJ. Acta Mat 1998;46:3109.

[28] Evans AG, Hutchinson JW, Ashby MF. Prog Mater Sci1998;43:171.

[29] Paul A, Ramamurty U. Mat Sci Eng A 2000; 281:1.

Figure Captions

Fig.1. Schematic of the constrained compression testing with steel sleeve. The aluminum block shown in the figure was used for compressing the foam inside the sleeve.

Fig. 2. Relative density distribution of all the samples tested.

Fig. 3. (a) Typical plots of the accumulated strain, ε_a, vs. number of fatigue cycles, *N*, with and without constraint. Here, both the specimens were tested such that the maximum stress of the fatigue cycle is 90% of the quasi-static plastic strength (obtained using Fig. 4(a) of Ref.12). Different regimes of fatigue in the closed-cell Al foam were delineated for the unconstrained case for the purpose of illustration. (b) Respective plots of the strain accumulation rate, $d\varepsilon_a/dN$ as a function of ε_a.

Fig. 4. Influence of maximum stress of the fatigue cycle, σ_{max} on the fatigue strain accumulation for the (a) unconstrained (b) constrained loading cases. Here, σ_{max} is normalized with the plastic strength, σ_p, estimated using curve fit in Fig. 4(a) of Ref. 12 and the measured relative density of the samples prior to fatigue loading. Solid lines in (a) are power law fits to the data whereas they are predicted variations in Fig. 4b.

Fig. 5. Effect of maximum stress of the fatigue cycle, σ_{max} on the fatigue strain accumulation rates, $d\varepsilon_a/dN$, plotted as a function of ε_a for the (a) unconstrained (b) constrained loading cases.

Fig. 6. Comparison of S-N curves for constrained and unconstrained specimens with an ε_a of (a) 4% and (b) 10% as criterion for strain to failure.

Fig.7. Scanning electron micrographs of foam cells taken after 4% deformation of the foam. Fig a, b) shows presence of fatigue cracks in cell walls c) buckle observed in a cell without many cracks under quasi-static compression d) fatigue striations observed at very large magnification on fracture surface of cracks. All the figures were obtained from samples tested with lateral constraint.

Fig. 8. Figure illustrating strain jumps in (a) unconstrained and (b) constrained specimens.

Fig. 9. Binarised images of the tomographs taken from a specimen subjected to quasi-static compression with lateral constraint to strain levels of (a) 0, (b) 6, (c) 12, (d) 21 and (e) 29%. Red circles highlight the selective deformation of large cell leading to collapse band formation. Fig. (f) shows the corresponding stress-strain plot with the interruption points marked.

Fig. 10. Binarised images of the tomographs taken from a sample that was fatigue loaded with constraint and interrupted at (a) 4, (b) 10, and (c) 15 % accumulated strains. Arrow marks in (a) indicates the onset of collapse band formation despite the presence of a large cell (highlighted by circle) in middle portion of the specimen. Note that this large cell does not deform even after 15% strain. It is also clear that collapse band formed in the top portion of the specimen and propagated towards lower portion. Fig. (d) shows the corresponding strain accumulation curve and interruption points.

Fig. 11. Compression of fatigued (up to 6% ε_a) samples showing (a) lower densification strain values compared to simply compressed specimens and (b) similar specific energy absorption values.

Fig. 12. Relative density profiles in different stages of samples tested in (a) quasi-static compression and (b) compression-compression fatigue loading. Since the specimen height decreases with straining, the profiles were rescaled to initial length of the specimen (100 mm) for comparison purpose. Note that the strains at interruption mentioned in Figs. 9 and 10 are higher than the strains mentioned in this figure because in the former are total strains (i.e., obtained when the samples are still under load) whereas the strains mentioned in Fig.12 are permanent accumulated strains.

Fig. 13. Variation of power law coefficient with normalized maximum stress.

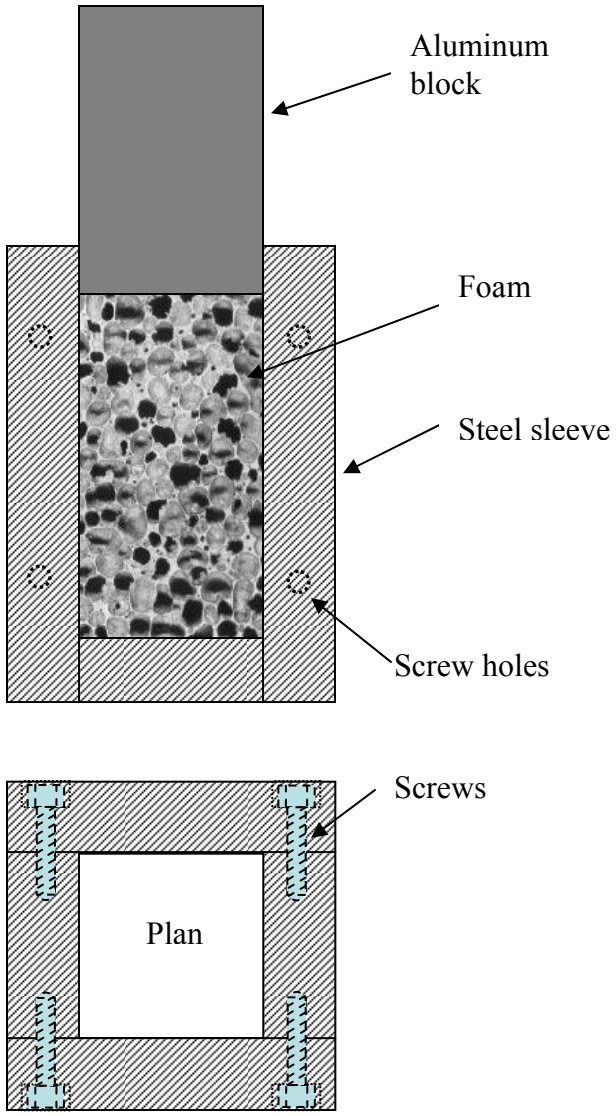

Fig.1. Schematic of the constrained compression testing with steel sleeve. The aluminum block shown in the figure was used for compressing the foam inside the sleeve.

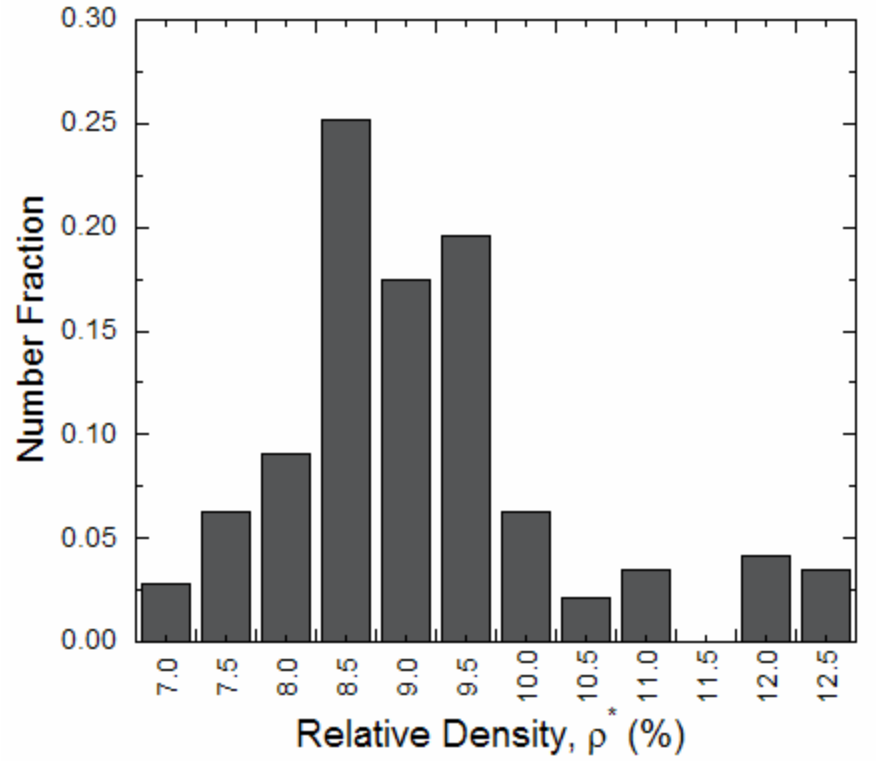

Fig. 2. Relative density distribution of all the samples tested.

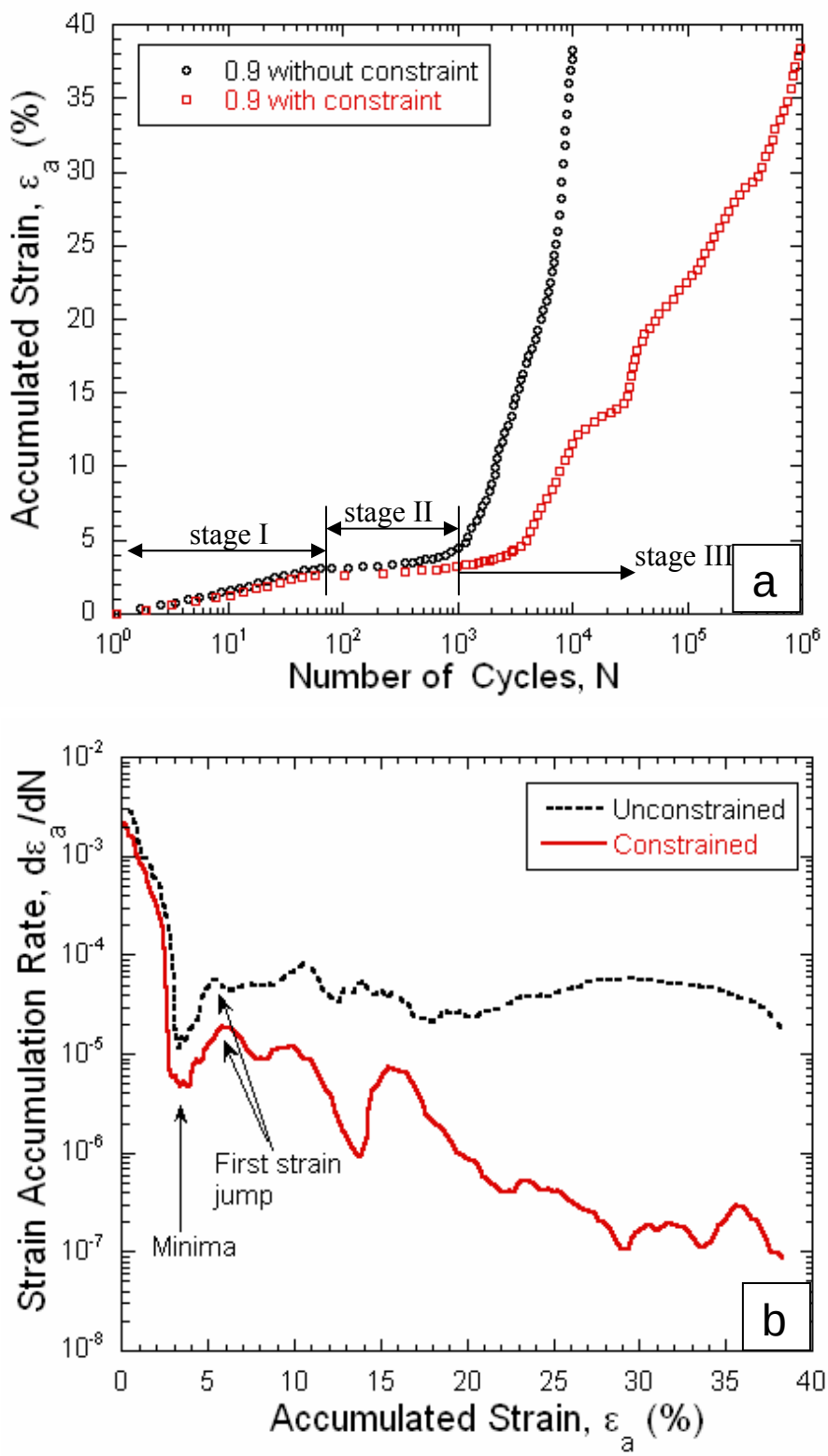

Fig. 3. (a) Typical plots of the accumulated strain, ε_a, vs. number of fatigue cycles, *N*, with and without constraint. Here, both the specimens were tested such that the maximum stress of the fatigue cycle is 90% of the quasi-static plastic strength (obtained using Fig. 4(a) of Ref.14). Different regimes of fatigue in the closed-cell Al foam were delineated for the unconstrained case for the purpose of illustration. (b) Respective plots of the strain accumulation rate, $d\varepsilon_a/dN$ as a function of ε_a.

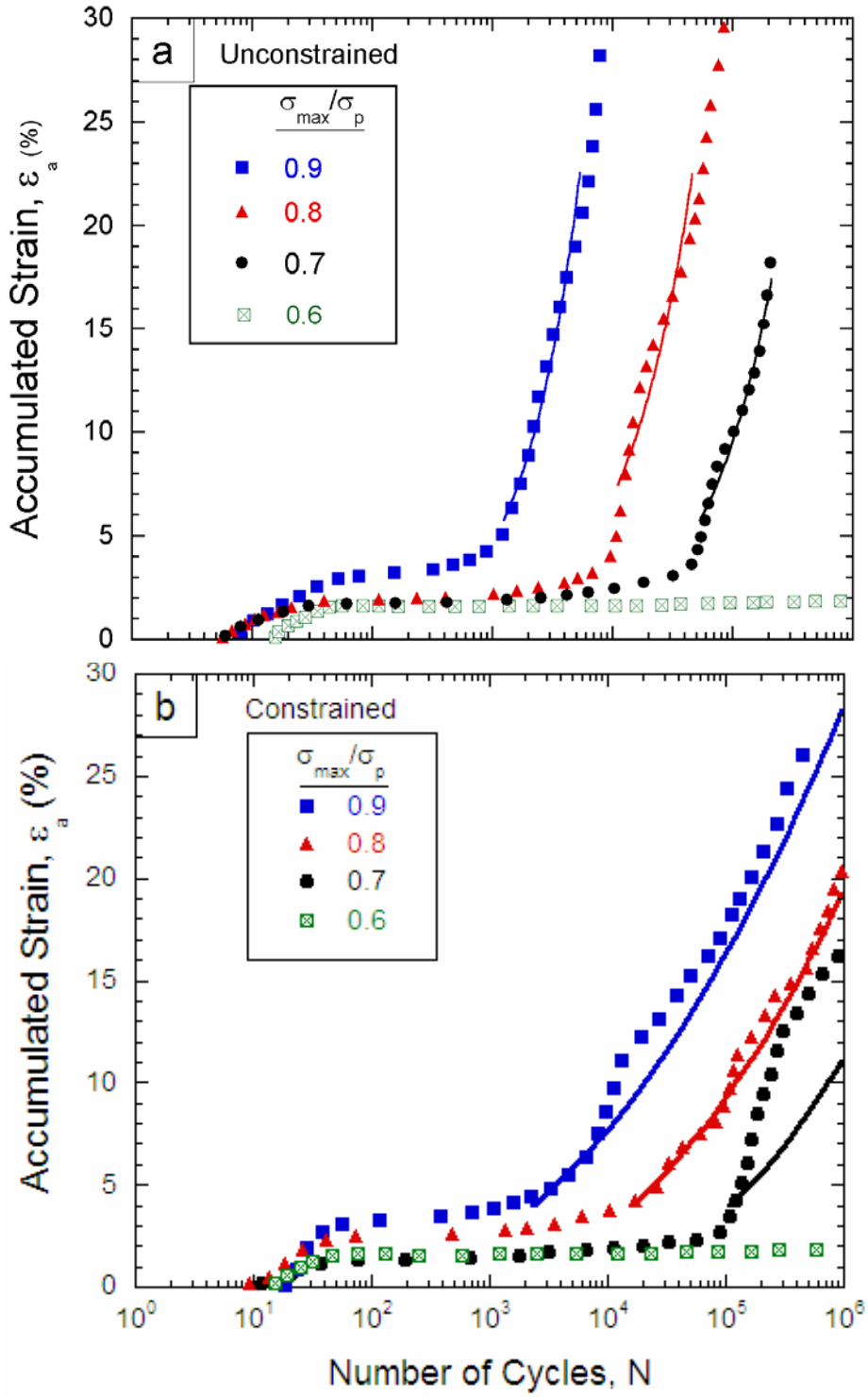

Fig. 4. Influence of maximum stress of the fatigue cycle, σ_{max} on the fatigue strain accumulation for the (a) unconstrained (b) constrained loading cases. Here, σ_{max} is normalized with the plastic strength, σ_p, estimated using curve fit in Fig. 4(a) of Ref. 14 and the measured relative density of the samples prior to fatigue loading. Solid lines in (a) are power law fits to the data whereas they are predicted variations in Fig. 4b.

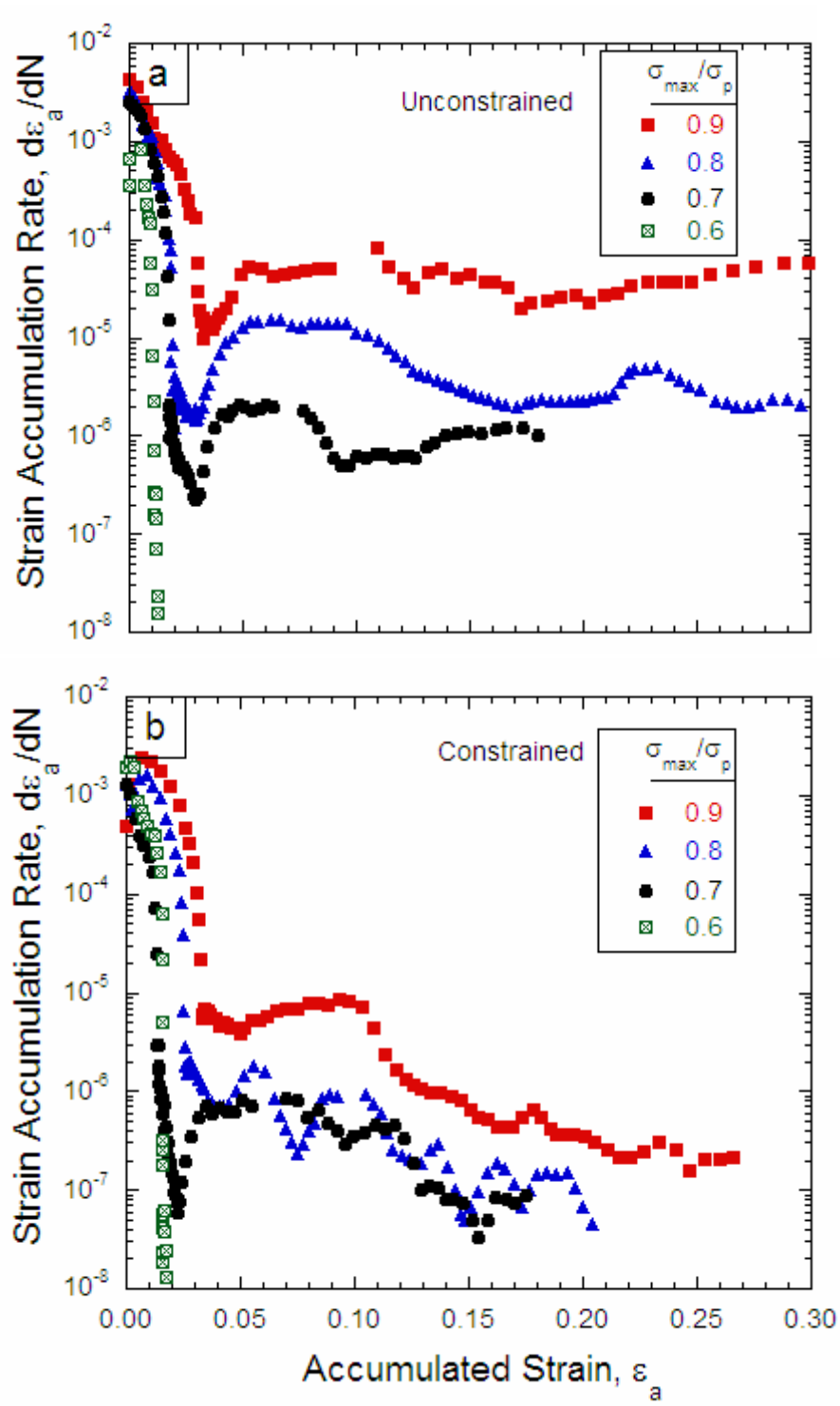

Fig. 5. Effect of maximum stress of the fatigue cycle, σ_{max} on the fatigue strain accumulation rates, $d\varepsilon_a/dN$, plotted as a function of ε_a for the (a) unconstrained (b) constrained loading cases.

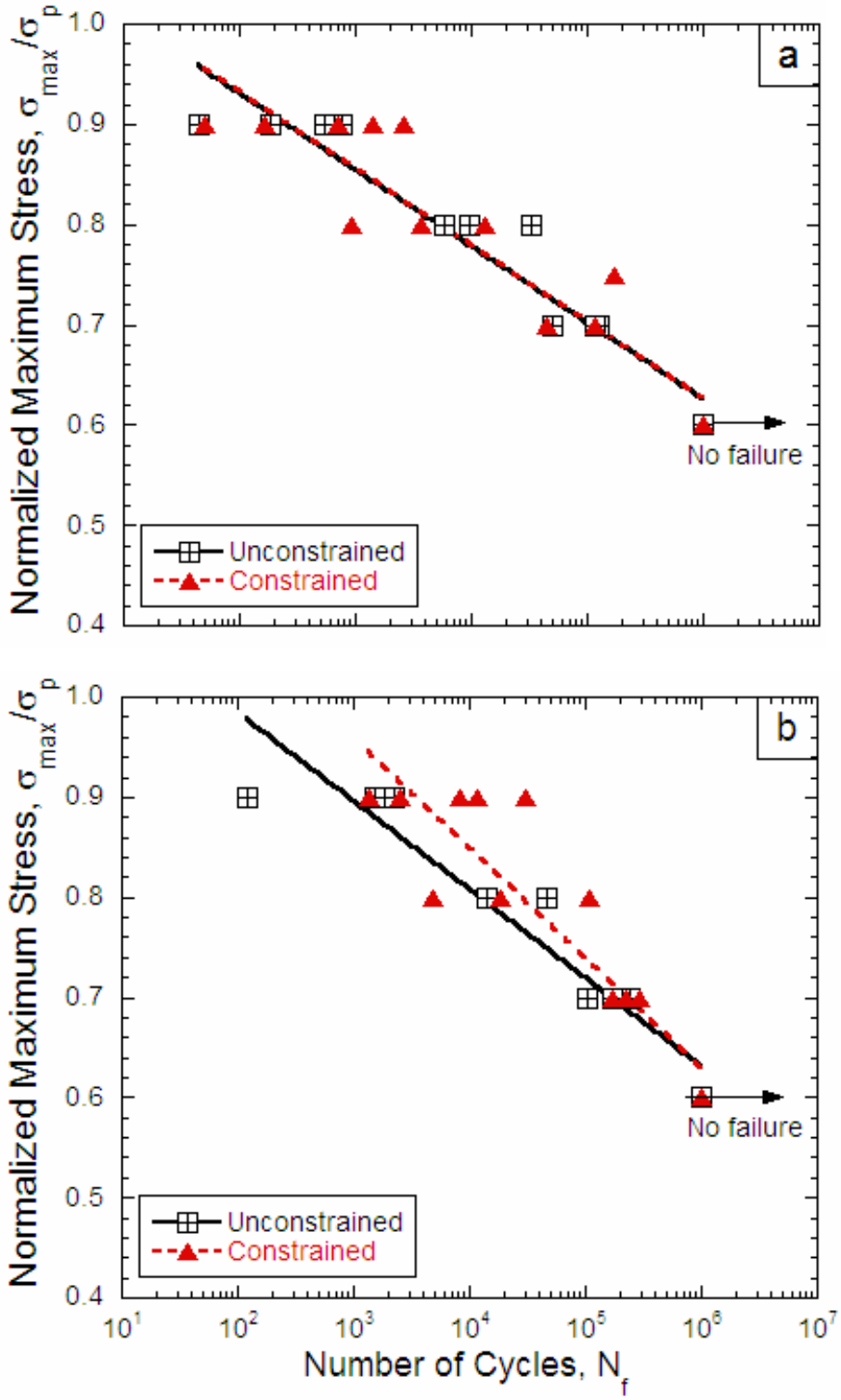

Fig. 6. Comparison of S-N curves for constrained and unconstrained specimens with an ε_a of (a) 4% and (b) 10% as criterion for strain to failure.

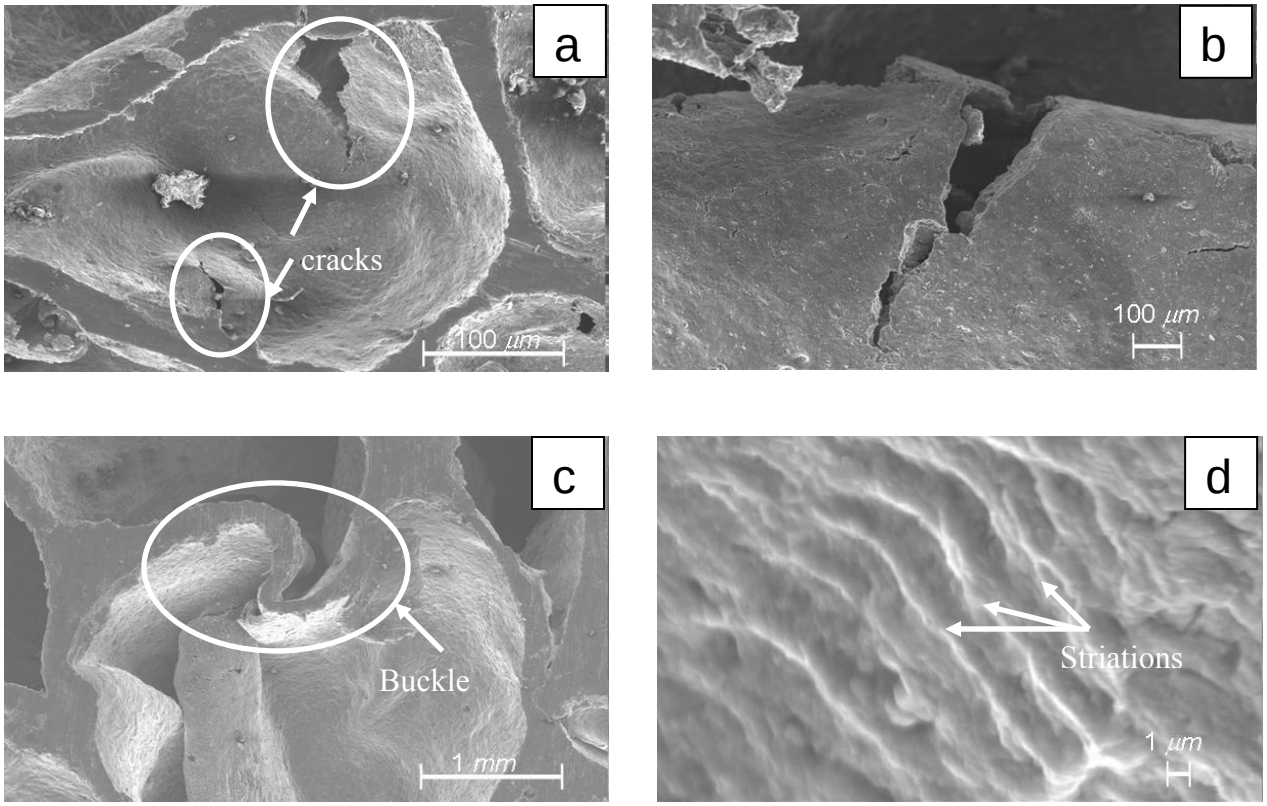

Fig.7. Scanning electron micrographs of foam cells taken after 4% deformation of the foam. Fig a, b) shows presence of fatigue cracks in cell walls c) buckle observed in a cell without many cracks under quasi-static compression d) fatigue striations observed at very large magnification on fracture surface of cracks. All the figures were obtained from samples tested with lateral constraint.

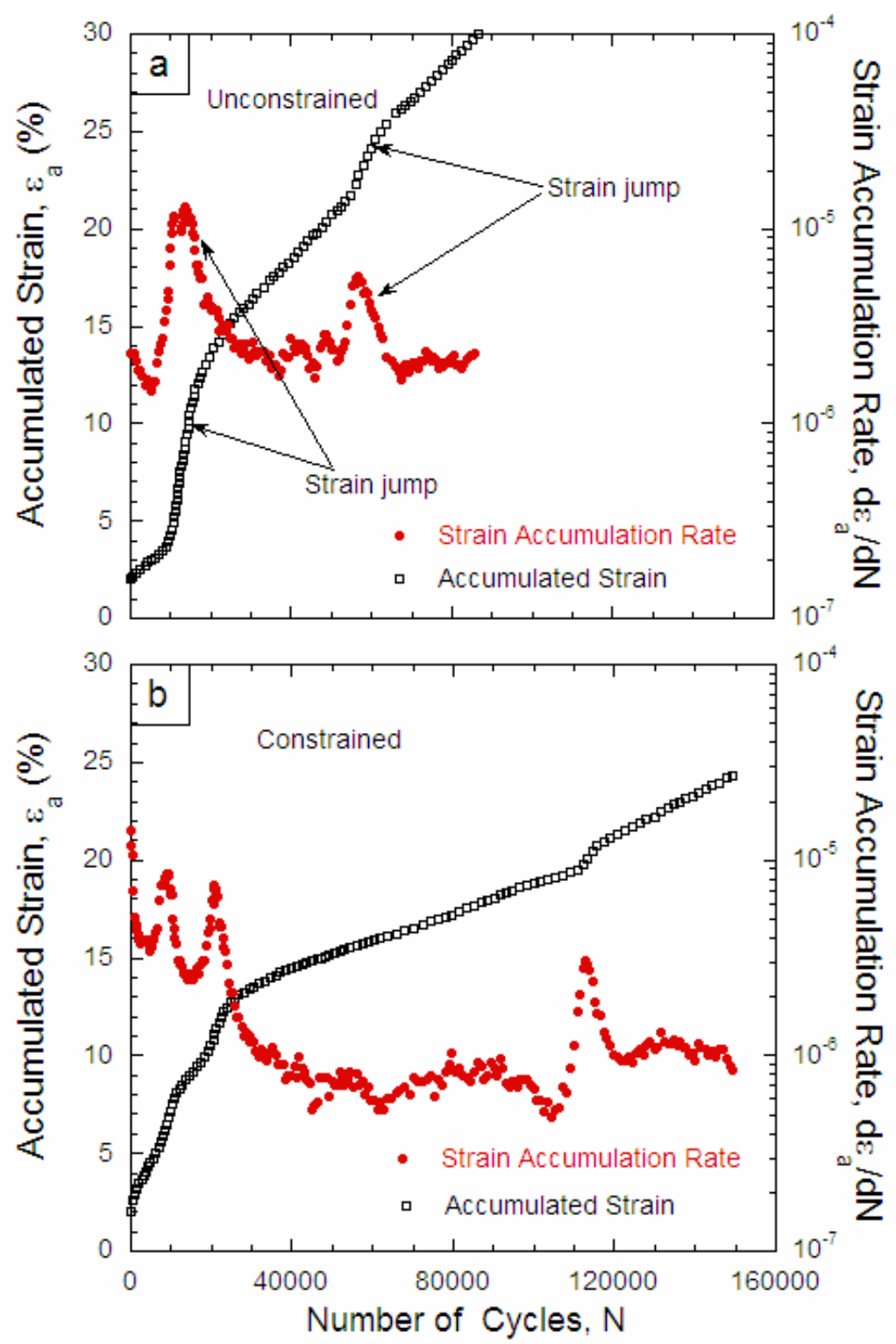

Fig. 8. Figure illustrating strain jumps in (a) unconstrained and (b) constrained specimens.

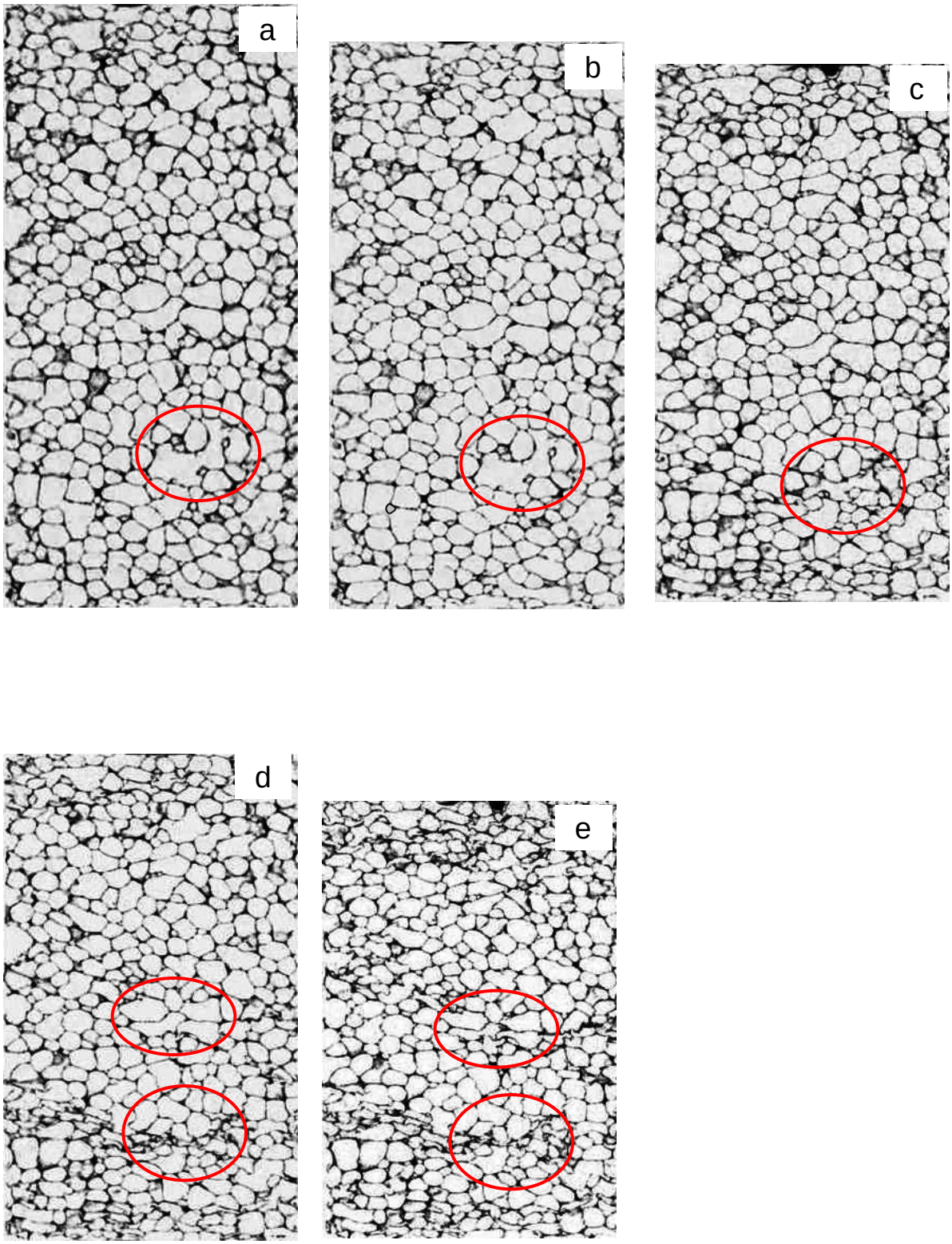
a
b
c
d
e

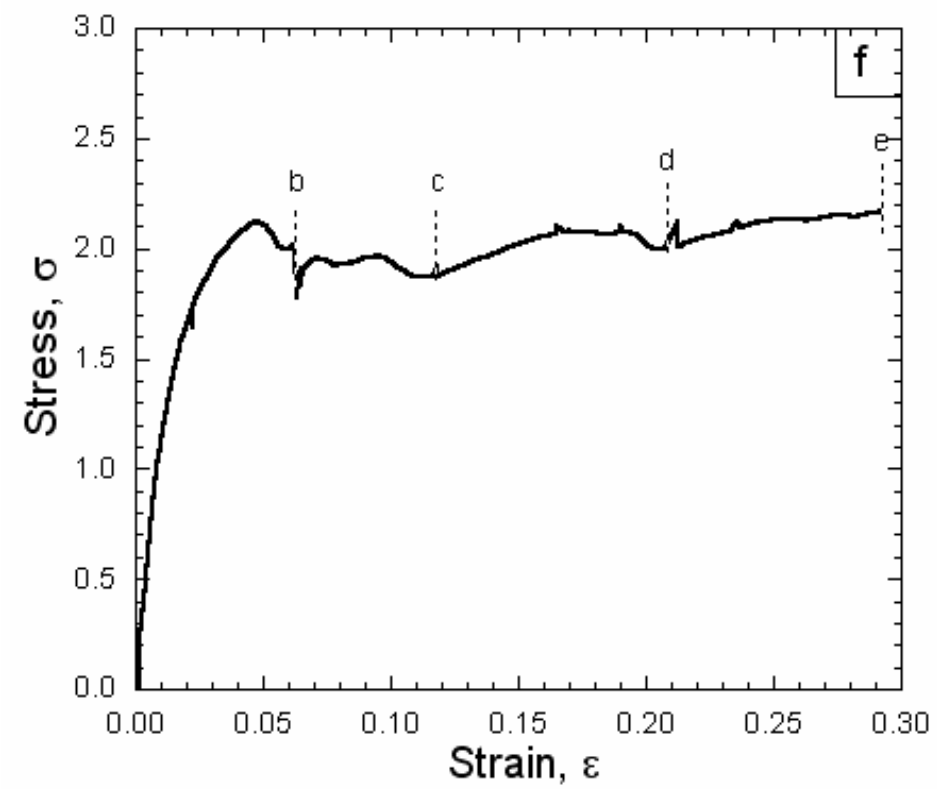

Fig. 9. Binarised images of the tomographs taken from a specimen subjected to quasi-static compression with lateral constraint to strain levels of (a) 0, (b) 6, (c) 12, (d) 21 and (e) 29%. Red circles highlight the selective deformation of large cell leading to collapse band formation. Fig. (f) shows the corresponding stress-strain plot with the interruption points marked.

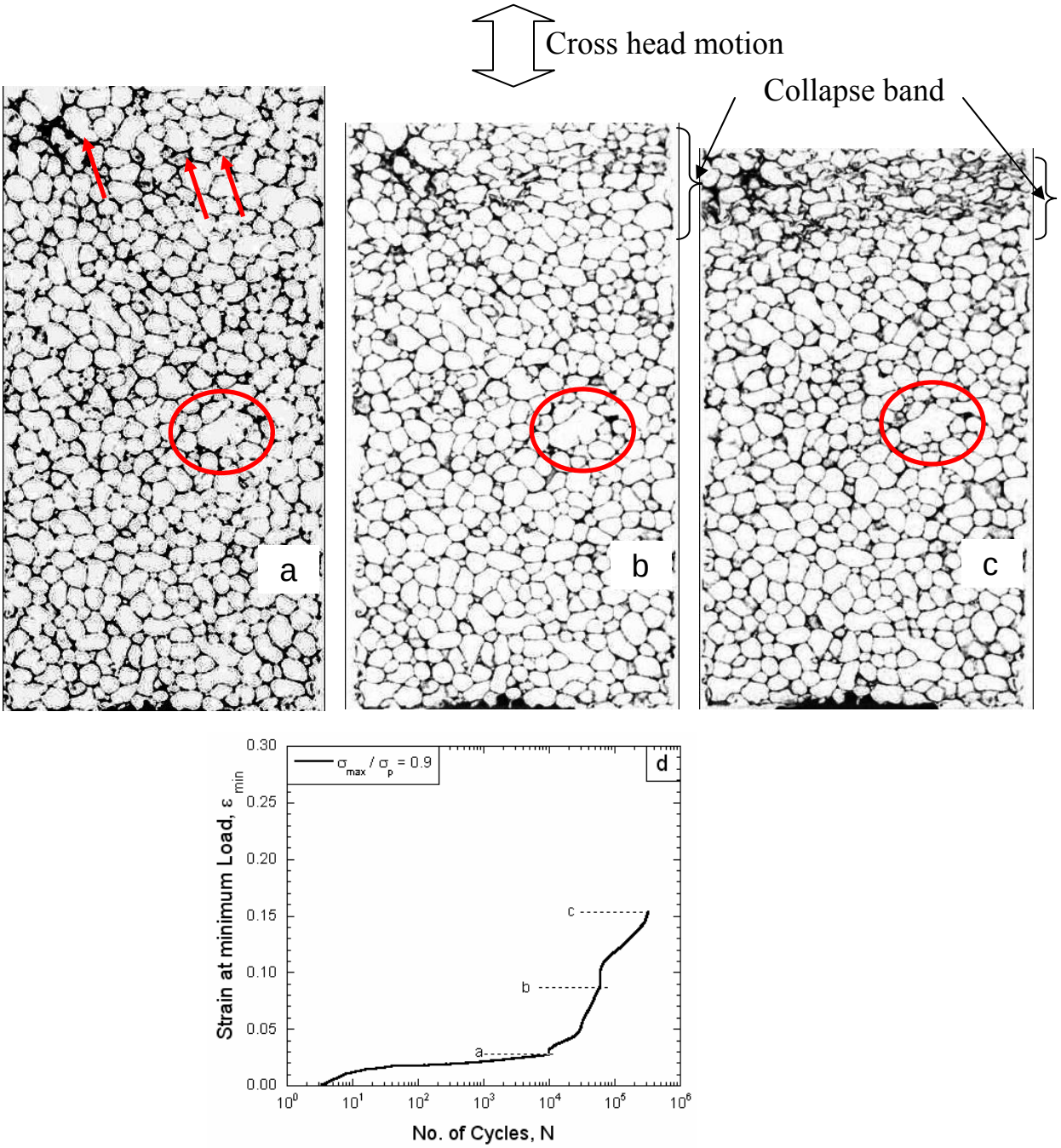

Fig. 10. Binarised images of the tomographs taken from a sample that was fatigue loaded with constraint and interrupted at (a) 4, (b) 10, and (c) 15 % accumulated strains. Arrow marks in (a) indicates the onset of collapse band formation despite the presence of a large cell (highlighted by circle) in middle portion of the specimen. Note that this large cell does not deform even after 15% strain. It is also clear that collapse band formed in the top portion of the specimen and propagated towards lower portion. Fig. (d) shows the corresponding strain accumulation curve and interruption points.

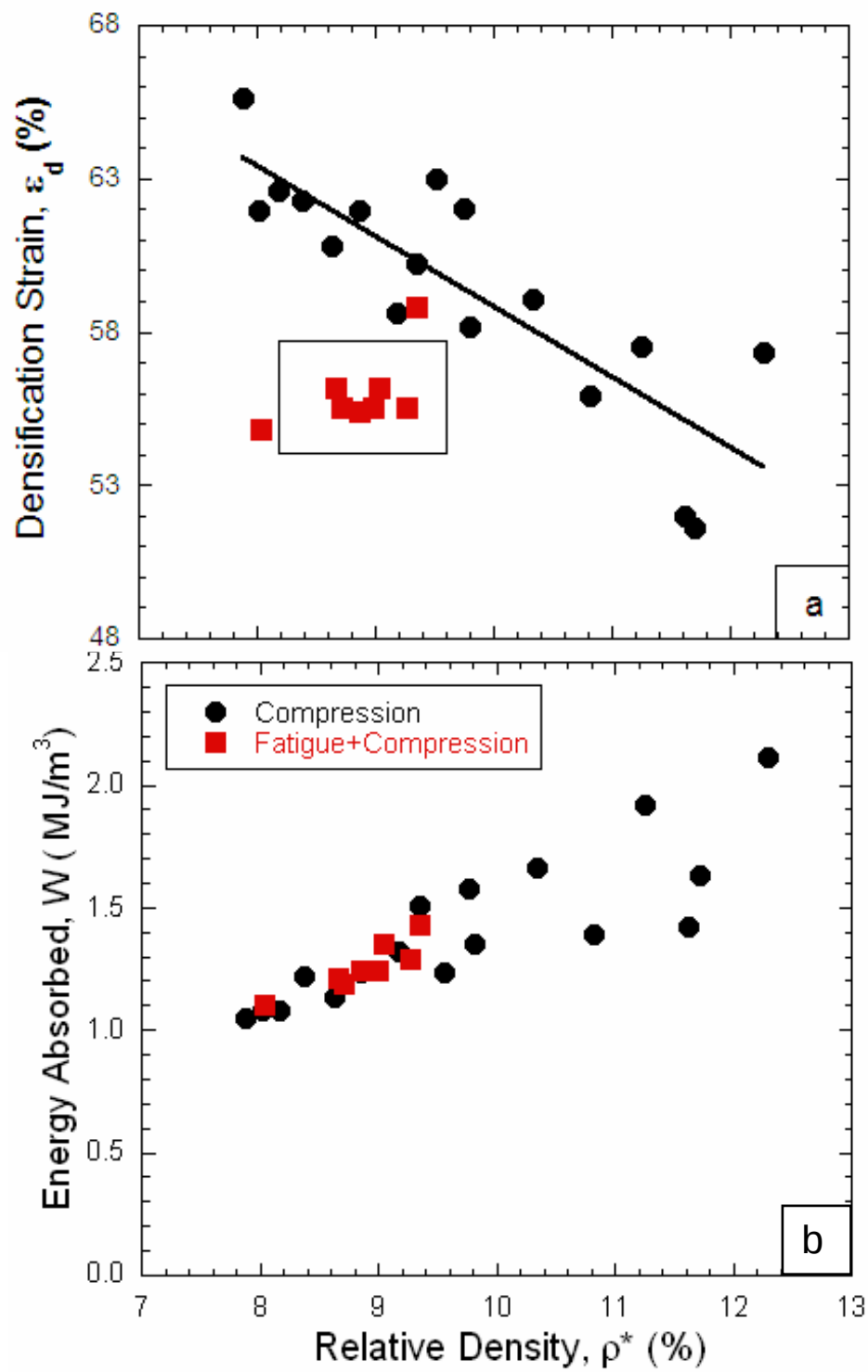

Fig. 11. Compression of fatigued (up to 6% ε_a) samples showing (a) lower densification strain values compared to simply compressed specimens and (b) similar specific energy absorption values.

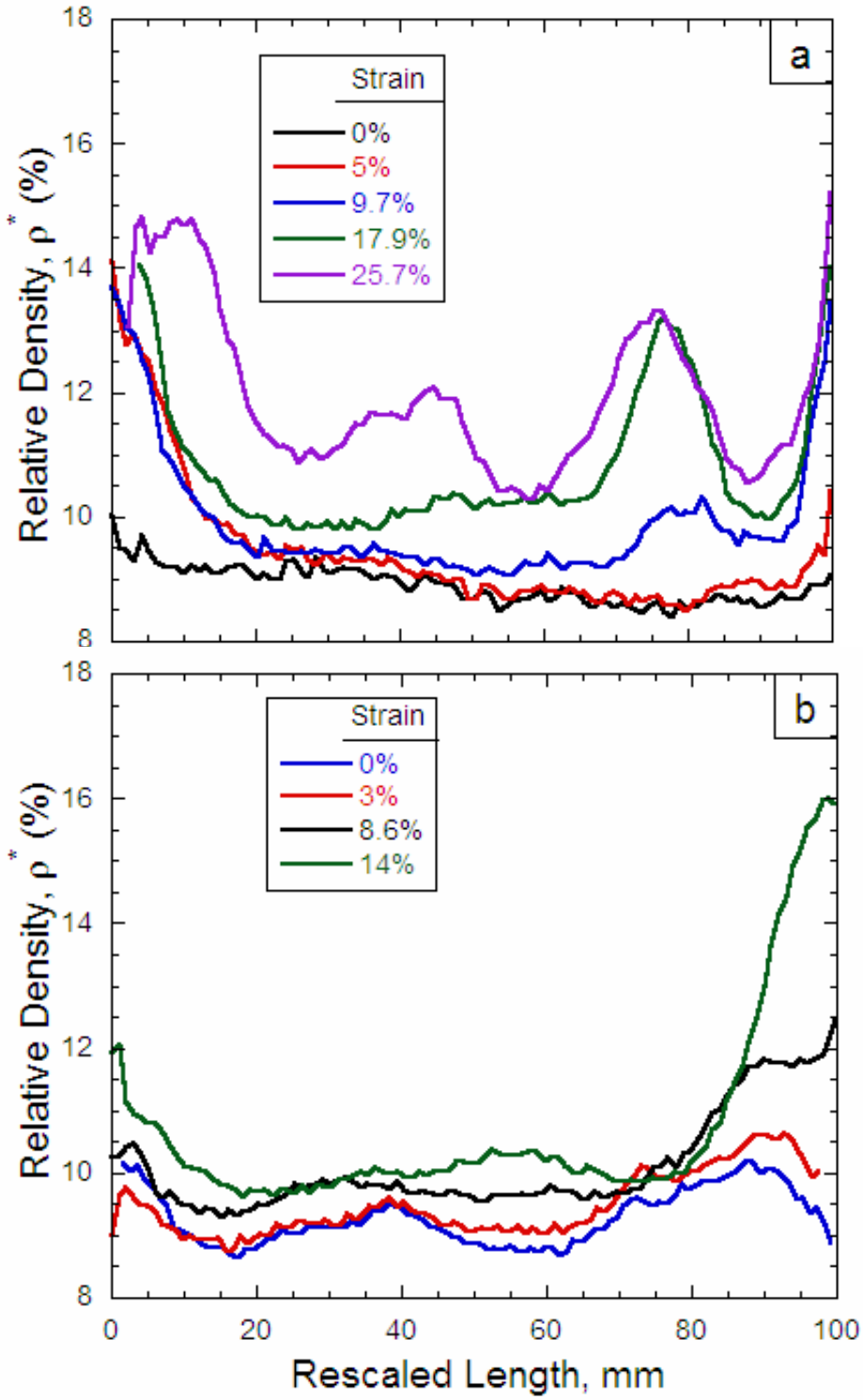

Fig. 12. Relative density profiles in different stages of samples tested in (a) quasi-static compression and (b) compression-compression fatigue loading. Since the specimen height decreases with straining, the profiles were rescaled to initial length of the specimen (100 mm) for comparison purpose. Note that the strains at interruption mentioned in Figs. 9 and 10 are higher than the strains mentioned in this figure because in the former are total strains (i.e., obtained when the samples are still under load) whereas the strains mentioned in Fig.12 are permanent accumulated strains.

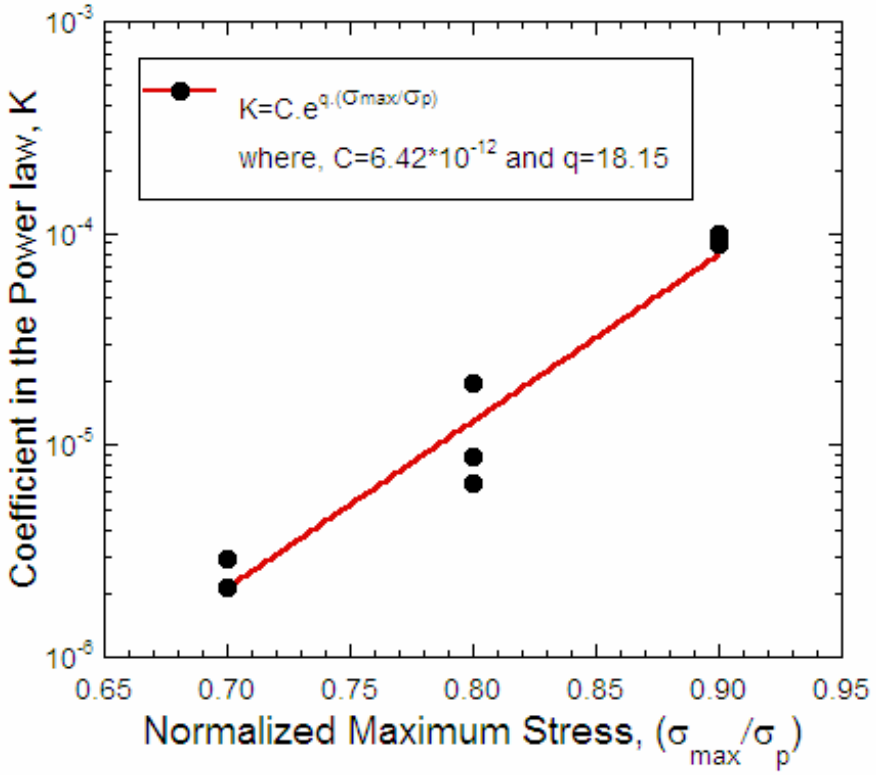

Fig. 13. Variation of power law coefficient with normalized maximum stress.